ARTICLE TYPE

Multi Scale Proper Generalized Decomposition based on the Partition of Unity[†]

Rubén Ibáñez[1,4] | Amine Ammar[2] | Elías Cueto[3] | Antonio Huerta[4] | Jean-Louis Duval[5] | Francisco Chinesta[1]

[1]ESI Group Chair @ PIMM - Procédés et Ingénierie en Mécanique et Matériaux, ENSAM ParisTech, 151 boulevard de l'Hôpital, Paris, France

[2]LAMPA, ENSAM Angers, 2 Boulevard du Ronceray, BP 93525, 49035 Angers Cedex 01, France

[3]Aragon Institute of Engineering Research, Universidad de Zaragoza, Edificio Betancourt. Maria de Luna, s.n., 50018 Zaragoza, Spain

[4]Laboratori de Calcul Numeric, Universitat Politecnica de Catalunya, BarcelonaTech, Calle Jordi Girona 1-3, 08034 Barcelona, Spain

[5]ESI Group, 3bis rue Saarinen, 94528 Rungis CEDEX, France

Correspondence
*Francisco Chinesta. Email:
Francisco.Chinesta@ensam.eu

Summary

Solutions of partial differential equations could exhibit a multi-scale behavior. Standard discretization techniques are constraint to mesh up to the finest scale in order to predict accurately the response of the system. The proposed methodology is based on the standard PGD rationale, thus, the PDE is transformed into a non-linear system that iterates between micro- and macro-scale states, where the time-coordinate could be viewed as a 2D-time, representing the micro and macro time scales. The macro scale effects are taken into account thanks to a FEM-based macro discretization whereas the micro-scale effects are handled with unidimensional parent spaces which are replicated throughout the domain. The proposed methodology can be seen as an alternative route to circumvent prohibitive meshes arising from the necessity of capturing fine scale behaviors.

KEYWORDS:
Partition of unity, Proper Generalized Decomposition, Time multi-scale.

1 | INTRODUCTION

Many problems in computational mechanics present a multi-scale behavior where the micro-scale effects influence the macro-scale ones and viceversa. Hence, the treatment of the different scales of the problem becomes very important to reach an accurate solution. Plenty of effort has been dedicated to deal with small scale effects either refining the mesh or introducing models that accounts for the subgrid effects. As a typical example, different levels of turbulence models can be found: e.g., Reynolds Averaged Navier-Stokes (RANS), Large-Eddy Simulation (LES) or Direct Navier-Stokes (DNS)[12]. In the solid domain, such a multi-scale behavior appears, for instance, in the spatial domain when dealing with meta-materials whose structure is defined at the micro level.

Several techniques have been applied throughout history, like the classic homogenization[21], that defines the micro-scale constitutive model in terms of a representative volume that satisfies the Hill-Mandel principle[14]. This methodology has proven to be very effective in order to circumvent the prohibitive computational cost of methods like FE^2. However, there is a strong hypothesis behind such homogenization technique, requiring a clear separation of scales between macro and micro effects.

Another way to handle these multi-scale effects is by using the variational multi-scale framework introduced by[28], where the effect of the micro-scale into the macro-scale variables is introduced in a consistent way developing different weak forms

associated with the macro and micro scales. This approach has been effectively applied in many problems such as the Navier-Stokes equation[29], among others.

Moreover, the multi-scale problem will appear when dealing with temporal evolutions that are composed by many harmonics at very different frequencies. Following standard time marching approaches, a suitable time step that captures the evolution of the finest scale has to be imposed, deriving into a prohibitive simulation cost. Many numerical algorithms have been proposed to dribble the time marching approach up to the finest time scale.

D. Neron et al.[26] proposed a numerical algorithm based on the LATIN-PGD able to handle temporal and spatial multi-scale behaviors appearing in solid mechanic problems. However, selecting the temporal macro basis just like the interfacial degrees of freedom coupling different macro domains is very problem dependent. The scalability of the methodology is restored via an appropriate correction of the temporal basis based on the residual.

F. Fritzen et al.[25,15] also partitioned the time domain into subintervals, where a common reduced basis is applied for all subintervals. Afterwards, additional interface restrictions have to be imposed to ensure continuity of the primal variable and her time derivative. Hence, variables at both extremes of each macro interval are set to zero, plus an offset calculated from the previous macro interval. Several viscoelastic problems are solved for various cyclic loading with varying frequency.

Y. Maday et al.[27,19] developed Parareal algorithm which also attempts to solve a temporal evolution iterating between macro and micro domain partitions so that the initial conditions for each micro interval are given by the macro resolution of the problem. The algorithm is also highly parallelizable, making it very efficient for either long time simulations or temporal problems involving many spatial degrees of freedom.

A. Ammar et al. in[2] proposed an efficient technique based on the separation of variables, where the time domain was partitioned into discrete subdomains following the standard PGD rationale[8,23,6,7], or equivalent reduced order approaches[1,13,5]. However, special attention had to be paid at the interfaces between discrete subdomains, where continuity was imposed by means of Lagrange multipliers.

A. Badias et al. in[4] developed an algorithm where the time domain was partitioned into different PGDs, but again the interface conditions between different subdomains could become a cumbersome task. Another numerical strategy based on combining different PGDs under the partition of unity (PU) rationale[30,3,20] was developed in[18]. The idea of using macro shape functions that respect the partition of unity allowed the method to combine different PGDs in a consistent manner. Moreover, the overlap between PGDs automatically solves the problem of interface compatibilities related to the not overlapped methodology. However, there may be situations in which the macro domain partition requires many PGDs to capture properly the behavior, reducing the scalability of the method.

The methodology proposed in this work aims to treat multi-scale problems by means of the separation of variables paradigm, where no need to impose a clear separation between scales is required. Indeed, the methodology is based on two main pillars: a generalization of the idea of time-domain partition, together with the overlapped multi-PGD framework. By doing that, the proposed methodology naturally inherits continuity between macro subdomains, clear extrapolation to higher dimensional spaces and scalability of the method even if the macro-domain partition is fine enough.

The paper is structured into four distinct sections. After this introduction, we introduce the theoretical description of the just developed method. In Section 3 we introduce a long list of numerical examples that show the potentialities of the proposed method. Finally, in Section 4 we draw some conclusions and explore the future research lines. Details of the implementation are given in the Appendix.

2 | BASICS OF THE METHOD

This section explains the main characteristics of the multi-scale PGD based on the partition of unity. The formulation is introduced for a one-dimensional variable first. Then, the formulation is extended to 2D problems and finally to time-multiscale problems.

Let us assume that a given function, $u(x)$, is the solution of a given partial differential equation. In terms of standard approximation basis, such as finite elements, it could be expressed as

$$u(x) = \sum_{i=1}^{N} N_i(x)u_i,$$ (1)

where N stands for the number of degrees of freedom used in the approximation of $u(x)$ or, in other words, the number of nodes in the mesh. Needless to say, $N_i(x)$ represent the standard finite element shape functions and u_i the nodal value of the sought function, if the employed approximation is interpolant.

However, if the solution presents a multi-scale approach, the mesh has to capture the details of the solution at the finest scale, thus deriving into a prohibitive simulation cost ($N \gg 1$). A possible way to circumvent this issue, within the PU paradigm, is to introduce a dependent variable that captures the solution details associated with the finest scale,

$$u(x) = \sum_{i=1}^{N} N_i(x)u_i \sum_{j=1}^{J} G_j(\tau(x - x_i))g_j, \tag{2}$$

where x_i is the centroid of the shape function $N_i(x)$, $\tau(x - x_i)$ is a dependent variable which presents an offset based on x_i, $G_j(\tau)$ is the j-th micro-scale shape function and g_j its associated micro-scale degree of freedom. Indeed, the micro-scale effects occurring in the compact support of the macro shape function $N_i(x)$ are going to be mapped into the same micro scale parent space, τ.

There are several ways to define the parent space. In the particular case where all macro shape function supports are identical, the easiest choice is to equal the length of the parent space with the length associated with the macro-scale shape function support, requiring only an off-set based on the centroid of the i-th macro-scale shape function. If the macro partition is not uniform, each macro-scale shape function support has to be mapped to the same reference parent space. Thus, the Jacobian of this mapping will appear in the definition of the τ variable. This particular case is not considered in the present work, that looks for the simplest and more general case, even if as considered later, it is not the most efficient. Future works will address adaptivity and consequently will consider this issue.

Remark 1. It is worth noting that in Eq. (2) macro degrees of freedom (u_i) and micro degrees of freedom (defining the local micro enrichment, g_j) are both unknown, in opposition to usual applications of PU where the enrichment functions are known and given a priori.

Fig. 1 shows the shape functions associated with both the macro (top) and the micro scale (bottom). Notice how a two-scale approach presents two meshes related to micro and macro scales, respectively. Indeed, each macro partition of the domain contributes to the parent micro scale and the parent micro space affects equally the macro partition. It is important to reckon that both macro and micro meshes are defined by the user. In order to improve the efficiency of the methodology, they should meet certain requirements as the ones listed below:

- The micro scale mesh should be defined in such a way that it captures the finest micro-scale behaviour. For instance, if the signal has a given maximum frequency, the micro scale mesh has to be defined in a way that this maximum frequency is well represented, according to the Niquist-Shanon sampling theorem. It is important also to highlight that refining the micro state mesh also could increase the number of fixed-point iterations between macro and micro scale states, as the non-linear system becomes bigger.

- The more a macro mesh is partioned, the simpler are the micro scale modes since the signal variation is captured by either the macro mesh or the micro mesh. Indeed, the more partitioned a macro mesh is, the more variation could be described only with the macro elements, letting less variation to be captured by the micro-scale mesh.

Moreover, it is worth mentioning the possibility of rewriting our solution function as $u(x, \tau)$, making it suitable for a PGD-like algorithm [9,16]. In this case, we proceed with a separation of variables as shown in Fig. 2 . Therefore, the initial one dimensional problem is transformed into a two dimensional problem. It is important to highlight that the macro mesh does not have to capture the solution of the finest scale, since it is handled by the micro scale mesh.
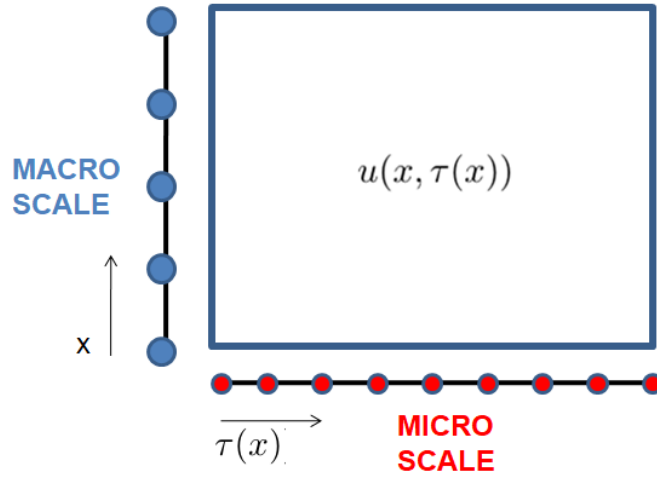
Thus, following a standard PGD rationale [10,11], the solution is sought in a Greedy manner through of a finite sum of M modal enrichments,

$$u(x, \tau) = \sum_{m=1}^{M} \sum_{i=1}^{N} N_i(x)u_i^m \sum_{j=1}^{J} G_j(\tau(x - x_i))g_j^m = \sum_{m=1}^{M} \sum_{i=1}^{N} N_i(x)u_i^m \mathbf{G}^T(\tau(x - x_i))\mathbf{g}^m = \sum_{m=1}^{M} u^m(x, \tau), \tag{3}$$

where the super-index m indicates the m-th PGD mode.
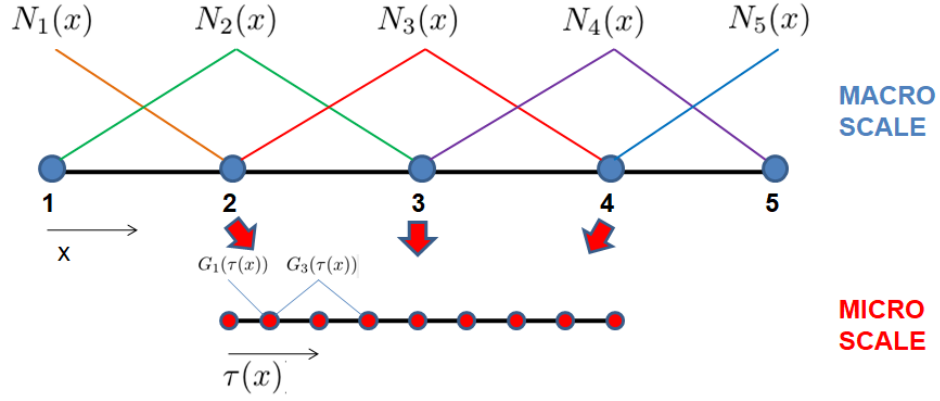
FIGURE 1 Shape functions of a multi-scale approach. Top, macro shape functions. Bottom, micro shape functions.

FIGURE 2 A separation of dependent variables, $u(x, \tau(x))$.

The discretization of a variational formulation by means of FEM, for instance, also needs an approximating space for the admissible variation of the field. In this particular case, when computing the M-th mode, we used a standard Galerkin projection

$$w^*(x, \tau) = \sum_{i=1}^{N} N_i(x) u_i^* \mathbf{G}^T(\tau(x - x_i)) \mathbf{g}^M + \sum_{i=1}^{N} N_i(x) u_i^M \mathbf{G}^T(\tau(x - x_i)) \mathbf{g}^*. \tag{4}$$

Nevertheless, SUPG or GLS stabilization can be also implemented in this formulation when dealing with highly convective (parabolic, in general) problems, see also [17].

Even if any linearization technique is possible, an alternated direction scheme is chosen in this work for solving the resulting nonlinear problem arising from the PGD rationale. Hence, when solving micro-scale modes, macro-scale admissible variations are set to zero (i.e., $u_i^* = 0$) and, conversely, when solving macro-scale modes, $\mathbf{g}^* = \mathbf{0}$.

Special attention needs to be paid when dealing with the derivatives of the approximation space, viz.

$$\frac{Du(x, \tau)}{Dx} = \frac{\partial u(x, \tau)}{\partial x} + \frac{\partial u(x, \tau)}{\partial \tau} \frac{\partial \tau}{\partial x} = \sum_{m=1}^{M} \sum_{i=1}^{N} \left(\frac{\partial N_i(x)}{\partial x} u_i^m \mathbf{G}^T(\tau) \mathbf{g}^m + N_i(x) u_i^m \frac{\partial \mathbf{G}^T(\tau)}{\partial \tau} \frac{\partial \tau}{\partial x} \mathbf{g}^m \right) \tag{5}$$

shows the application of the chain rule in order to account for the dependance of $\tau(x - x_i)$. For the sake of simplicity, the dependance of τ with respect to x coordinate will be set to one, as we are analyzing the case in which the parent space length
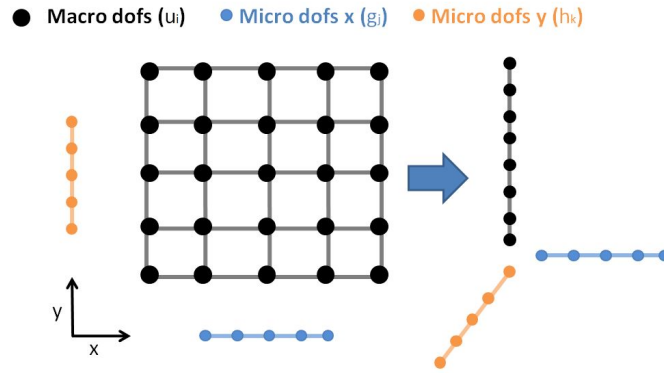
FIGURE 3 A separation of dependent variables in a 2D space, $u(\mathbf{x}, \tau_x, \tau_y)$.

coincides with each one of the macro scale shape function support length, otherwise the Jacobian of the transformation should be used.

The same rationale can be easily applied to higher dimensional spaces. Imagine that a 2D case (i.e., $\mathbf{x} = (x, y)$) is approximated by means of a 2D macro mesh and the details of the micro scale are given by one-dimensional modes acting along each spatial direction. Hence, the approximation space will read

$$u(\mathbf{x}, \tau_x, \tau_y) = \sum_{m=1}^{M} \sum_{i=1}^{N} N_i(\mathbf{x}) u_i^m \mathbf{G}^T(\tau_x) \mathbf{g}^m \mathbf{H}^T(\tau_y) \mathbf{h}^m, \tag{6}$$

where $\mathbf{g}^m$ and $\mathbf{h}^m$ are the degrees of freedom of the m-th PGD mode acting on x and y subscales, respectively. Indeed, u_i adopts the same role than in the 1D case, since it will be responsible of weighting the subgrid behavior throughout the domain.

The separated representation by means of partition of unity-based PGD in higher dimensions is depicted in Fig. 3 . Note that an initial 2D problem is transformed into a 3D problem, where one dimension takes into account the macro variations of the solution, whereas the other two dimensions take into account the subgrid scales taking place along x and y directions, respectively. It is very important to notice that subgrid scales are going to propagate throughout the entire domain, being the macro mesh the responsible of controlling the propagation of the subgrid behavior.

It is also important to highlight that the proposed approach reduces the amount of degrees of freedom required to handle subgrid scales in comparison with standard multigrid methods [24]. Imagine that a 2D domain is partitioned using a coarse regular mesh composed of $D_x \times D_y$ linear elements. Let us assume that each element is refined even more to handle subgrid scales using a mesh of $d_x \times d_y$ linear elements. The typical size of the entire system will be $D_x \times D_y \times d_x \times d_y$. Nevertheless, the proposed methodology is able to handle subgrid scales at a computer cost proportional to $M((D_x \times D_y) + d_x + d_y)$. Indeed, if the number of modes required to represent the solution does not grow too much (i.e., $M = \mathcal{O}(10)$), computing subgrid scales becomes affordable.

3 | NUMERICAL EXAMPLES

In this section, several numerical examples based on the multi-scale PGD formulation are tested. The first part shows the convergence of the method for three different one-dimensional cases. The second part shows several examples of the proposed methodology for different two-dimensional cases.

Following standard procedures in the PGD rationale, two stopping criteria are required: the first one stops the alternated direction (or fixed point) scheme within the m-th mode computation step, and is required to solve the non-linearity arising from the separation of variables. A second stopping criteria is required to stop computing new modes. In this analysis, we have defined these two stopping criteria as

$$\mathcal{E}_{fp}^{m,i-1} = \sqrt{\frac{\int_{\Omega}(u^{m,i} - u^{m,i-1})^2 d\Omega}{\int_{\Omega}(u^{m,i})^2 d\Omega}} < tol_{fp}, \tag{7}$$

and

$$\mathcal{E}_{mode}^m = \sqrt{\frac{\int_\Omega (u^m)^2 d\Omega}{\int_\Omega (u^1)^2 d\Omega}} < tol_{mode}, \tag{8}$$

where superindex m stands for m-th mode and superindex i is related to the i-th fixed point iteration.

3.1 | One-dimensional numerical examples

In this first section we analyze three different toy problems in one dimension. These include approximation, diffusion and convection problems.

3.1.1 | Multiscale approximation of a given function

This first example concerns the approximation of a function that shows multiscale features. Since we deal with an approximation case, there is no governing partial differential equation in this problem. In other words, a given function $f(x)$ is to be approximated by means of a multi-scale approximation $u(x, \tau)$. The weighted residual form associated with this problem reads

$$\int_\Omega w^*(x, \tau) u(x, \tau) dx = \int_\Omega w^*(x, \tau) f(x) dx \quad \forall \, x \in \Omega = [0, 1]. \tag{9}$$

In this case the function to approximate is defined as

$$f(x) = \frac{x \cos(8\pi x)}{8\pi}. \tag{10}$$

Fig. 4 shows the reconstructed solution (red line) versus the reference solution (blue line) when the macro domain is partitioned using 5 degrees of freedom (black dots), i.e., $N = 5$. The micro domain is partitioned using 80 linear finite elements, i.e., $J = 81$. As it can be noticed, the macro partition coincides exactly with the period of the signal, which is precisely the reason why only 1 mode ($M = 1$) is required to accurately represent the solution. Indeed, the micro scale mode is giving us the cosine signal whereas the macro scale is taking care of the linear growth.
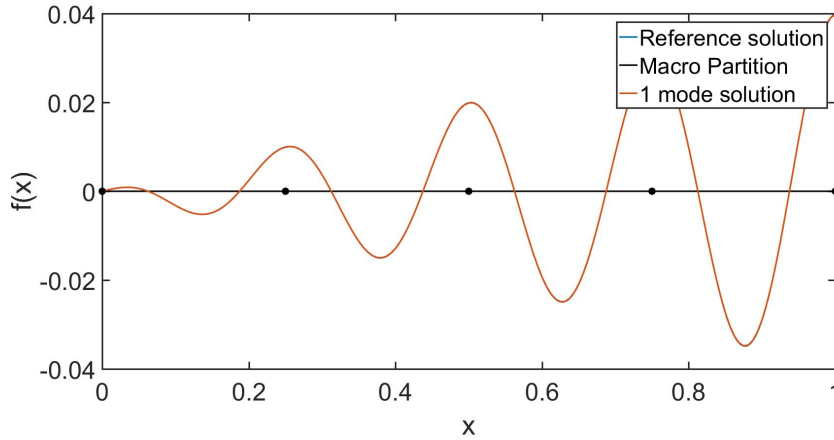

FIGURE 4 Approximation problem. The reconstructed solution with one single mode is represented by the red line. The reference solution is the blue line. In this case, the macro-domain partition employed 5 degrees of freedom, represented as black dots.

Fig. 5 shows the relative error in logarithmic scale between the reconstructed solution and the reference solution as a function of PGD modes for the 1D approximation case with macro domain partition coincident with the signal period. Note how, with only 1 mode, the multiscale PGD presents a low relative error. The same can be appreciated if the weight of the different PGD modes are compared, the first mode is almost four orders of magnitude bigger than the other two.
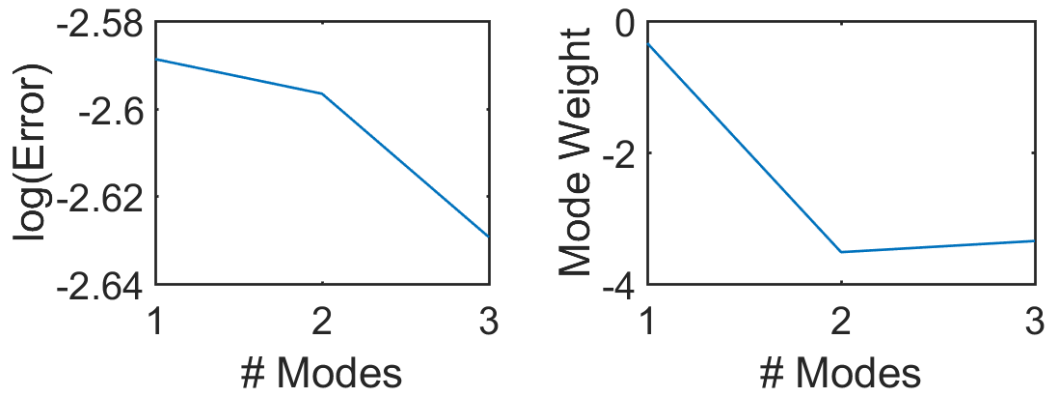
FIGURE 5 1D approximation problem macro partition coincident with signal period. Left, relative error with respect to the reference solution as a function of the number of PGD modes. Right, weight of each computed PGD mode.
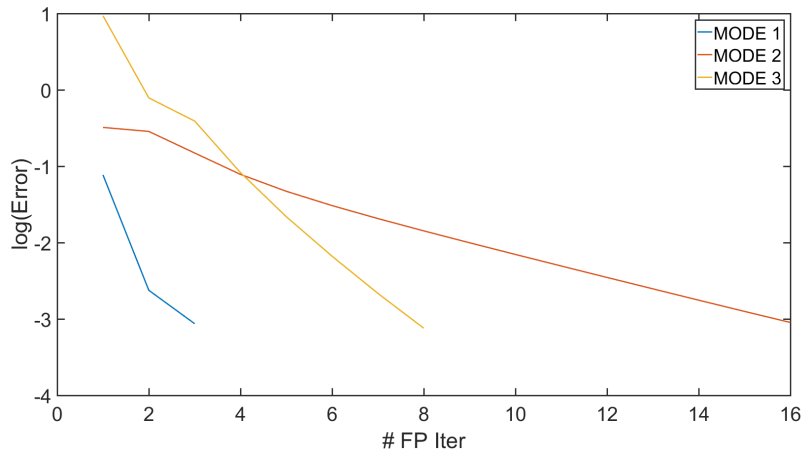

FIGURE 6 Alternate direction scheme convergence for the 1D approximation case with macro partition coincident with signal period.

Fig. 6 shows the convergence of the alternated direction algorithm for each one of the modes in the 1D approximation case with macro domain coincident with the signal period. As it can be seen, all modes present a fast convergence till the stopping criterion $1e − 3$, being the first mode the fastest one.

However, the exact period of our signal is not known a priori in most cases. Therefore, convergence of the method when the macro partition does not coincide with the signal period is checked as well. Fig. 7 shows the reconstructed solution (red line) against the reference one (blue line) when the macro domain partition does not coincide with the signal period. The top figure, involves a reconstructed solution with one mode, whereas the bottom one involves five modes. It is important to notice that the one-mode solution captures the main trend of the signal. However, there are some regions where the signal is not properly captured. Indeed, the solution involving five modes reproduces the reference signal very accurately.

Fig. 8 shows the relative error in logarithmic scale with respect to the reference solution as a function of the PGD modes for the 1D approximation case where the macro domain is not coincident with the signal period. The method converges monotonically towards the reference solution. The same decay can be appreciated comparing the weight of different PGD modes.

Fig. 9 shows the convergence of the alternated directions algorithm for each one of the modes in the 1D approximation case with macro domain non coincident with the signal period. As it can be seen, all modes present a reasonable convergence till the stopping criterion $1e − 3$, being the first mode the fastest one. The convergence of the fixed point wherever the macro mesh is
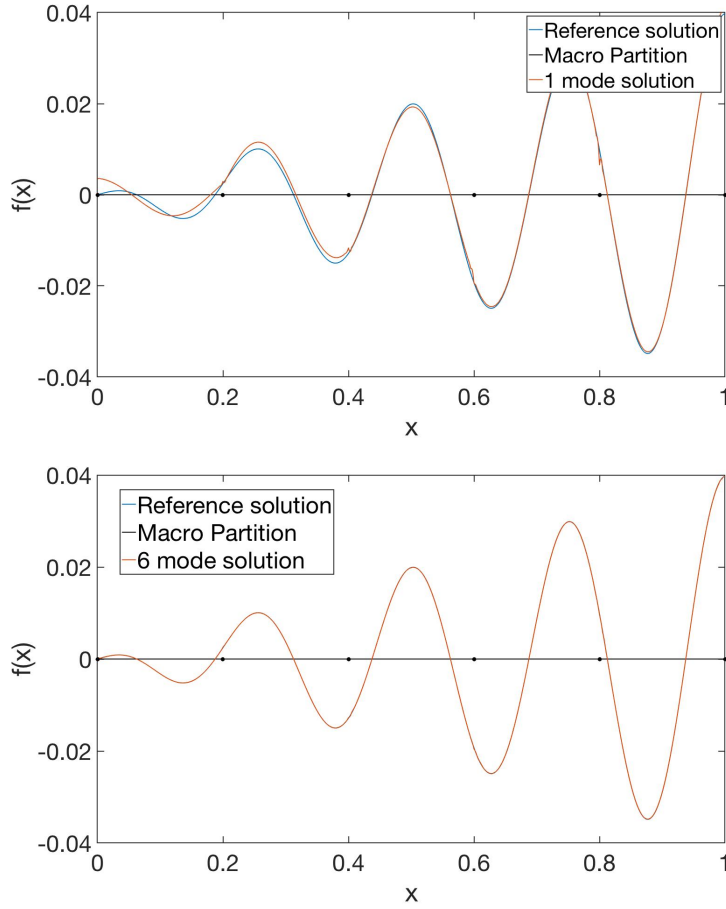
FIGURE 7 Approximation problem. Top: solution with one single mode. Bottom: 6 modes. The reconstructed solution appears as a red line. The reference solution is represented by a blue line. Macro-domain partition with 6 degrees of freedom, appearing as black dots.

not coincident with the signal period becomes slower compared with the coincident case. This is expected, since the functions found by the PGD algorithm are harder to capture in the non coincident case.

3.1.2 | Diffusion Case

The second test problem is a pure diffusion equation. The weak form related to this problem is

$$\int_\Omega \frac{Dw^*(x,\tau)}{Dx} \frac{Du(x,\tau)}{Dx} dx = \int_\Omega w^*(x,\tau(x)) f(x) dx, \quad \forall\, x \in \Omega = [0,10]. \tag{11}$$

The chain rule is required, as in Eq. (5), due to the dependence of τ with respect to x. The source term and the two boundary conditions ensuring that the problem is well posed are
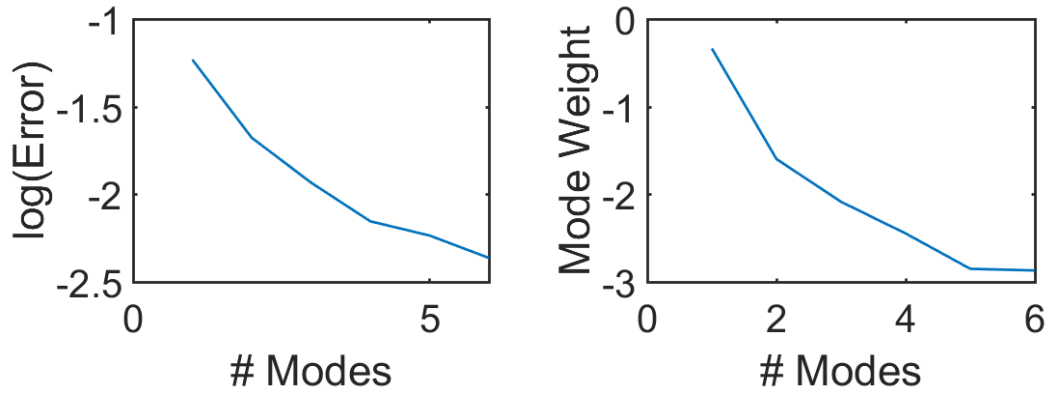
$$f(x) = \cos(2\pi x) + \frac{x}{100}, \tag{12}$$

$$u(0) = 0, \tag{13}$$

$$u(10) = 0. \tag{14}$$
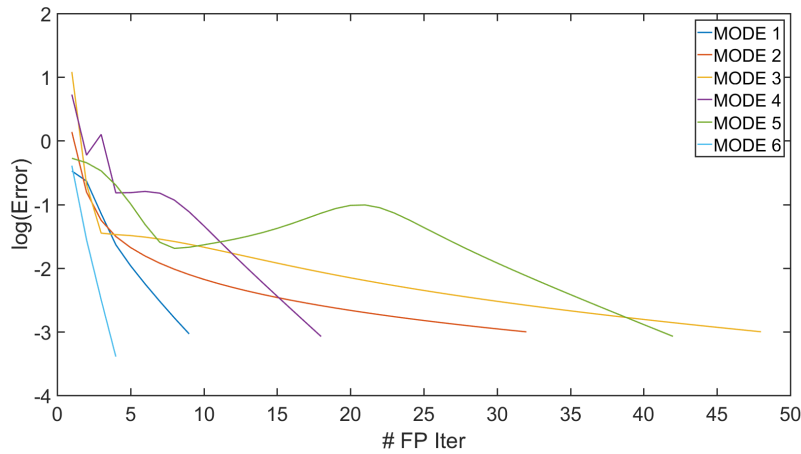
Under these conditions, the analytical solution of the problem reads

$$u(x) = \frac{\cos(2\pi x) - 1}{4\pi^2} + \frac{x}{6} - \frac{x^3}{600}. \tag{15}$$

FIGURE 8 1D approximation problem macro partition non coincident with signal period. Left, relative error with respect to the reference solution as a function of the number of PGD modes. Right, weight of each computed PGD mode.

FIGURE 9 Alternate direction scheme convergence for the 1D approximation case with macro partition non coincident with signal period.

Fig. 10 compares the reconstructed solution using the first PGD mode against the reference solution. The macro domain has been partitioned using 8 degrees of freedom. As it can be noticed, the first mode already captures the macro behavior, however, extra modes are required to identify the oscillatory behavior of the micro scale. Indeed, the reconstructed solution with 3 modes already captures the oscillations of the micro scale.

Fig. 11 shows both the convergence of the reconstructed solution with respect to the number of PGD modes and the weight of each PGD mode. Again, results show good convergence properties towards the reference, exact solution. Note how the weight of subsequent mode decreases monotonically.

Fig. 12 shows the convergence of the alternated direction algorithm for each one of the modes in the 1D diffusion case. It can be appreciated how the fixed point converges properly for each one of the modes.
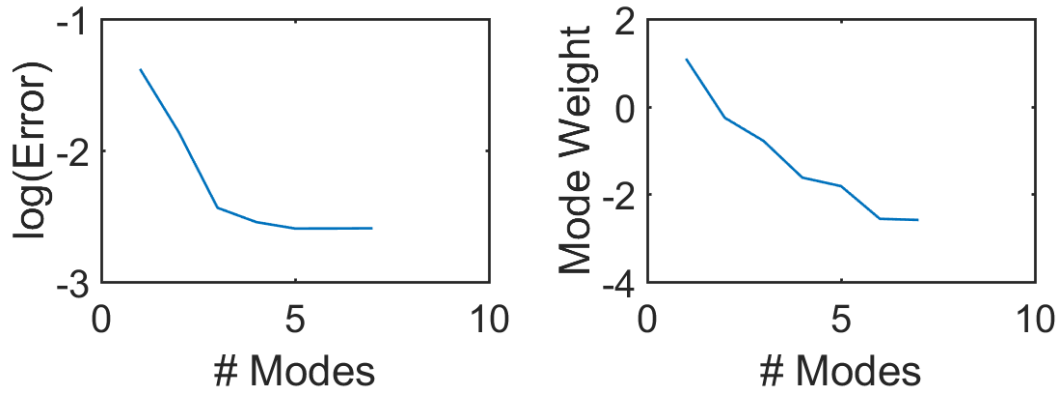
3.1.3 | Convection Case

The third example is a convection problem, whose weak form reads

$$\int_{\Omega} w^*(x, \tau(x)) \frac{Du(x, \tau(x))}{Dx} dx = \int_{\Omega} w^*(x, \tau(x)) f(x) dx \quad \forall\, x \in \Omega = [0, 10]. \tag{16}$$
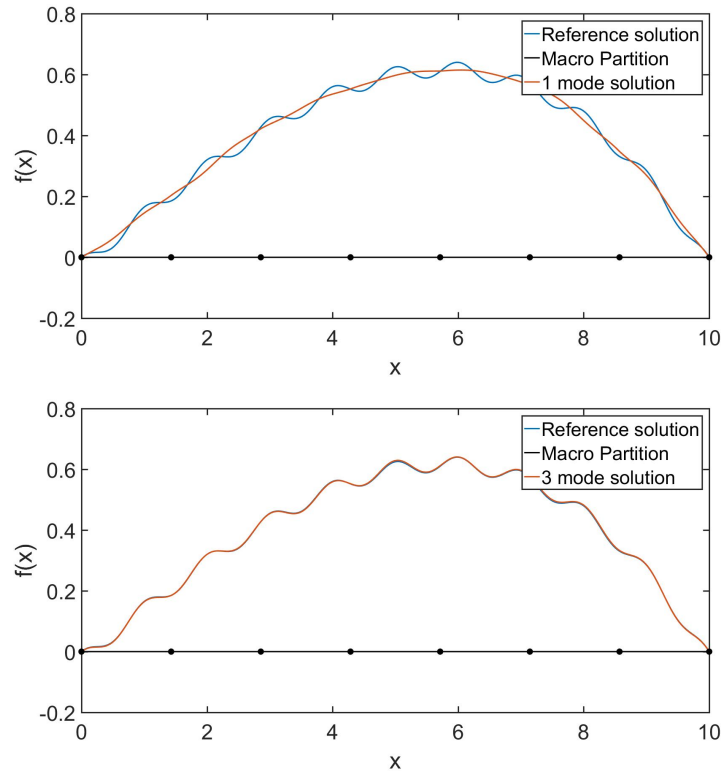
FIGURE 10 Diffusion problem. Top, 1 mode. Botoom, 3 modes. Reconstructed solution, red line. Reference solution, blue line. Macro domain partition with 8 degrees of freedom, black dots.


FIGURE 11 1D diffusion problem. Left, relative error with respect to the reference solution as a function of the number of PGD modes. Right, weight of each computed PGD mode.

It is well-known that special attention has to be paid when dealing with convection-dominated equations to ensure convergence. A standard streamline-upwind Petrov-Galerkin (SUPG) is implemented in this particular case [12]. Therefore, the test function is defined as

$$w^*(x, \tau(x)) = u^*(x, \tau(x)) + \beta \frac{Du^*(x, \tau(x))}{Dx}, \tag{17}$$

where β is a numerical coefficient controlling the stabilization of the numerical scheme. It is important to notice that the numerical scheme remains consistent since the test function affects both sides of Eq. (16).
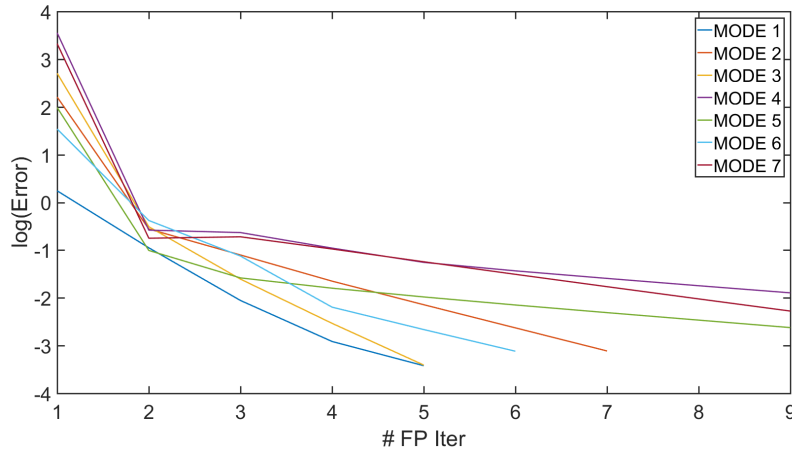
FIGURE 12 Alternate direction scheme convergence for the 1D diffusion case.

The source term of the problem is

$$f(x) = x \sin(12\pi x) + \frac{x}{30}, \tag{18}$$

while the initial condition (left boundary) is taken as

$$u(0) = 0. \tag{19}$$

In that case, the analytical solution satisfying this initial value problem is

$$u(x) = \frac{\sin(12\pi x)}{144\pi^2} - \frac{x \cos(12\pi x)}{12\pi} + \frac{x^2}{60}. \tag{20}$$

Fig. 13 shows the reconstructed solution involving one (top) and seven (bottom) modes versus the reference one. The macro domain has been partitioned using 9 degrees of freedom. As it can be noticed, the reconstructed solution is far from the reference one, when only one mode is involved. However, the PGD algorithm converges towards the reference solution when more modes are added into the approximation.

In turn, Fig. 14 shows the convergence of the multi-scale PGD algorithm for the 1D convection case. The method converges well, reaching a relative error of 10^{-4} when using 7 modes. It is important to notice that the error seems to stagnate after 5 PGD modes. Of course, by refining the macro scale the error decreases.

Fig. 15 shows both the convergence of the reconstructed solution with respect to the number of PGD modes and the weight of each PGD mode for the 1D convective case. Again, the methodology shows good convergence properties towards the reference, exact solution. Analyzing more in detail the mode weights, the first four modes are of the same order of magnitude whereas the rest of them experiences a monotonic decay. The absence of monotonic decay in the mode weights is not surprising since, as proved in classic PGD references, it is only guaranteed when solving symmetric, positive definite operators.

Fig. 16 shows the convergence of the alternated direction algorithm for each one of the modes in the 1D convective case. It can be appreciated how the fixed point converges properly for each one of the modes. However, its convergence may be slow in some particular modes.

3.2 | Two dimensional numerical examples

This section extends the analysis of the developed methodology to three different two-dimensional cases: approximation, diffusion and convection-reaction-diffusion problems.
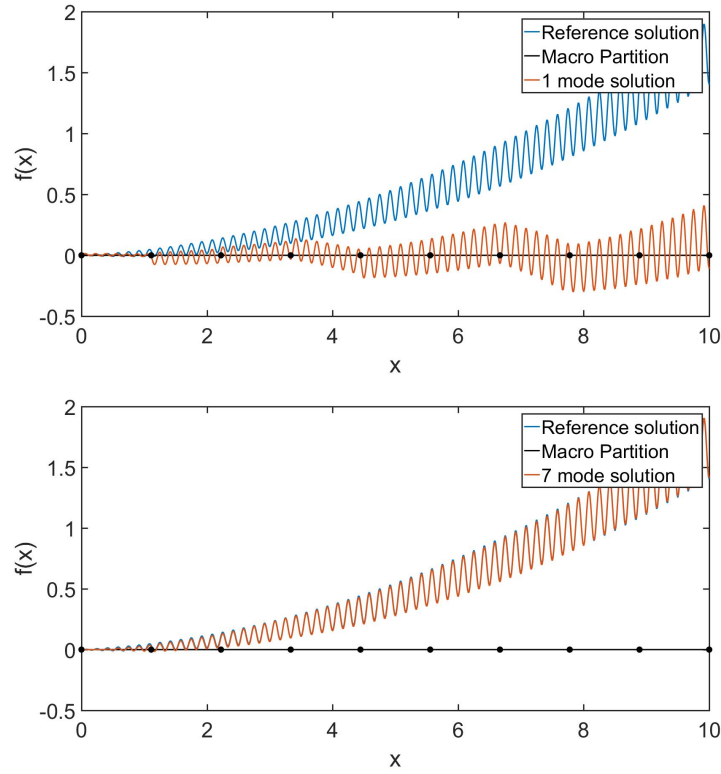
FIGURE 13 Convection case. Top, 1 mode. Botoom, 7 modes. The reconstructed solution is represented as a red line, while the reference solution appears in blue line. Macro domain partition with 10 degrees of freedom, represented as black dots.
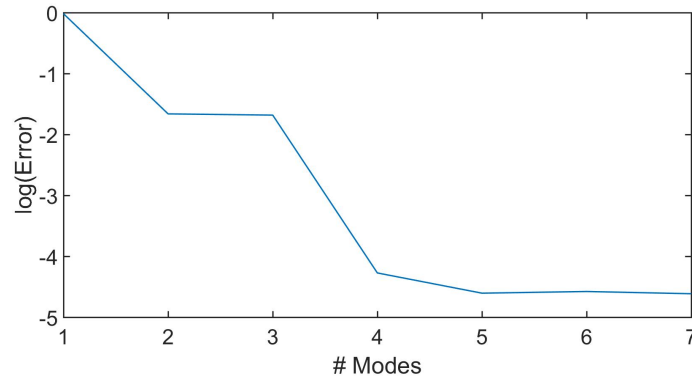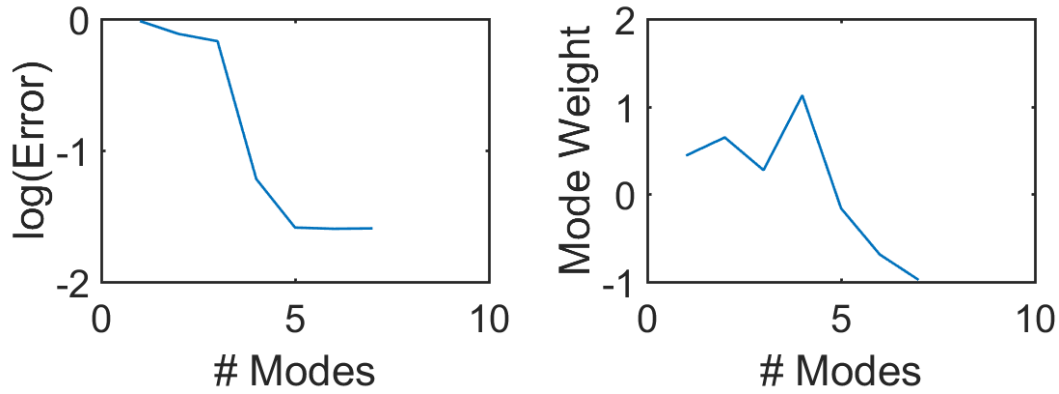

FIGURE 14 Relative error of the reconstructed solution with respect to the reference solution as a number of PGD modes for the convection case.

3.3 | 2D approximation problem

Again, we consider the multiscale approximation of a given function $f(\mathbf{x})$ by a sought function $u(\mathbf{x})$. The weighted residual (Bubnov-Galerkin) form of this problem is

$$\int_\Omega w^*(\mathbf{x}, \tau_x, \tau_y) u(\mathbf{x}, \tau_x, \tau_y) d\mathbf{x} = \int_\Omega w^*(\mathbf{x}, \tau_x, \tau_y) f(\mathbf{x}) d\mathbf{x} \quad \forall \, \mathbf{x} \in \Omega = [0, 1]^2 \tag{21}$$

FIGURE 15 1D diffusion problem. Left, relative error with respect to the reference solution as a function of the number of PGD modes. Right, weight of each computed PGD mode.
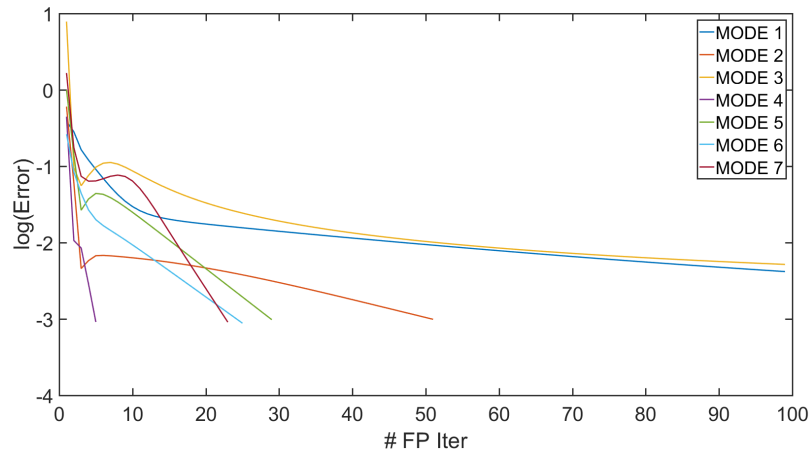
FIGURE 16 Alternate direction scheme convergence for the 1D convection case.

In this case we consider a function

$$f(\mathbf{x}) = x\cos(8\pi x)y\cos(8\pi y). \tag{22}$$

Note that no boundary conditions need to be imposed for this problem.

Fig. 17 shows the analytical solution (left) versus the reconstructed solution using the multi-scale PGD algorithm with 3 modes. The macro domain has been partitioned using a mesh of 25 degrees of freedom, since each spatial direction has been partitioned using 5 nodes. As it can be clearly seen, the reconstructed solution captures the main features of the reference solution. The small differences are due to the fact that the partition of the macro domain does not coincide with the period of the signal. Therefore, extra modes will be required to alleviate this non conformity.

Fig. 18 shows the convergence plot associated with the 2D approximation case as a function of the modal enrichments of the solution. Two kinds of indicators are shown: the left plot indicates the L2 relative error of the multi-scale PGD solution with respect to the reference solution in logarithmic scale, whereas the right plot shows the L2 norm of each multi-scale PGD mode also in logarithmic scale. Note the monotone convergence of the solution just like the monotonic decay in the norm of the modes.

Fig. 19 shows the convergence of the alternated direction algorithm for each one of the modes in the approximation case. As it can be seen, all modes present a fast convergence till $1e-2.5$. Afterwards, all modes are still converging but the convergence slope is decimated.
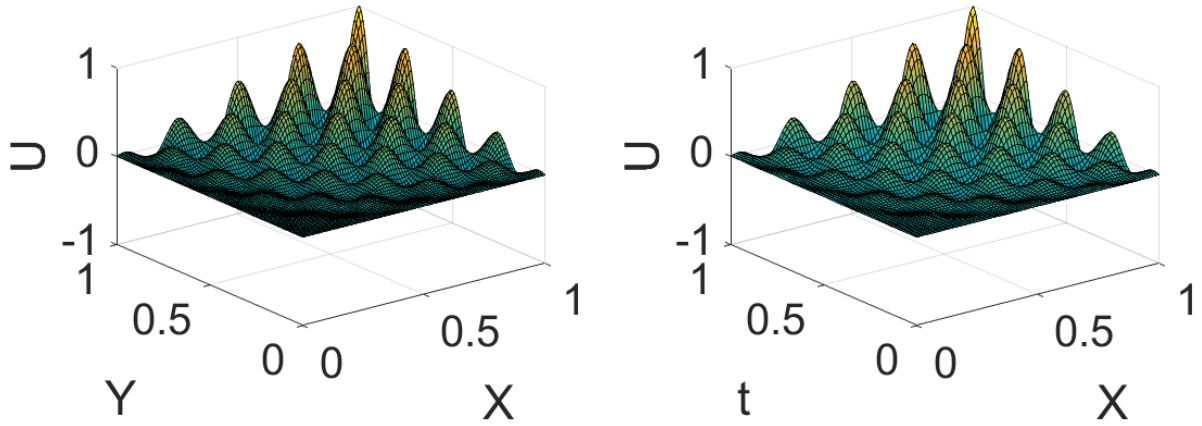
FIGURE 17 2D Approximation case. Left: reference solution. Right: reconstructed solution. Macro domain partitioned with $5 \times 5 = 25$ degrees of freedom.
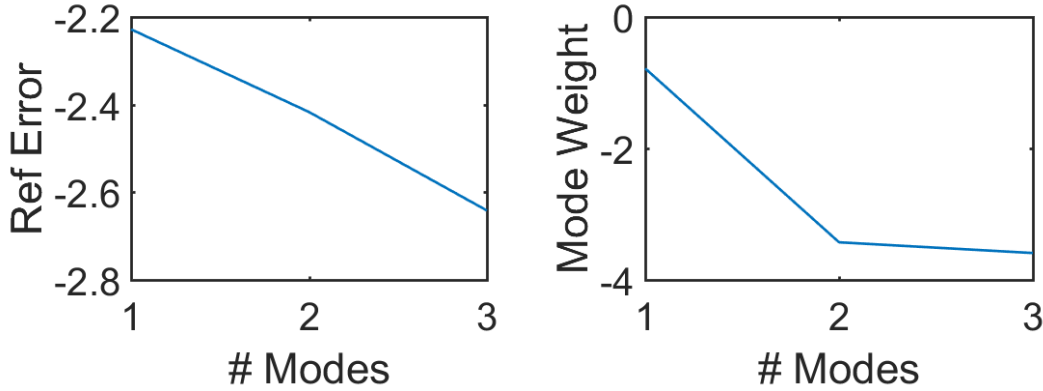
FIGURE 18 2D Approximation case. Left, L2 relative error of the reconstructed solution with respect to the reference solution. Right, L2 norm for each multi-scale PGD modes.

3.4 | 2D diffusion case

The weak form of this diffusion problem is

$$\int_{\Omega} \frac{Dw^*(\mathbf{x}, \tau_x, \tau_y)}{D\mathbf{x}} \cdot \frac{Du(\mathbf{x}, \tau_x, \tau_y)}{D\mathbf{x}} d\mathbf{x} = \int_{\Omega} w^*(\mathbf{x}, \tau_x, \tau_y) f(\mathbf{x}) d\mathbf{x} \quad \forall \, \mathbf{x} \in \Omega = [0, 1]^2. \tag{23}$$

with boundary conditions

$$u(0, y) = u(1, y) = u(x, 0) = u(x, 1) = 0. \tag{24}$$

The chain rule is required, as shown in Eq. (5), due to the dependence of τ_x and τ_y with respect to x and y, respectively. The source term f considered in this case was

$$f(\mathbf{x}) = 2w^2 xy \sin(wx) \sin(wy) - 2wx \sin(wx) \cos(wy) - 2wy \cos(wx) \sin(wy). \tag{25}$$

In this particular case, the angular velocity is set to $w = 20\pi$. In that situation, the analytical solution is given by

$$u(x, y) = x \sin(wx) y \sin(wy). \tag{26}$$

It is important to highlight the treatment of the boundary conditions in order to solve the diffusion problem. Vanishing Dirichlet boundary conditions need to be imposed on the boundary, so that all macro degrees of freedom placed at the boundary are fixed
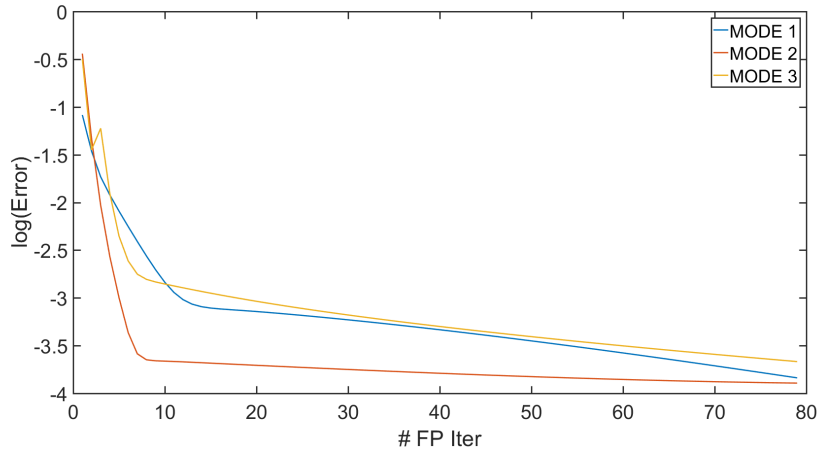
FIGURE 19 Alternate direction scheme convergence for the 2D approximation case.
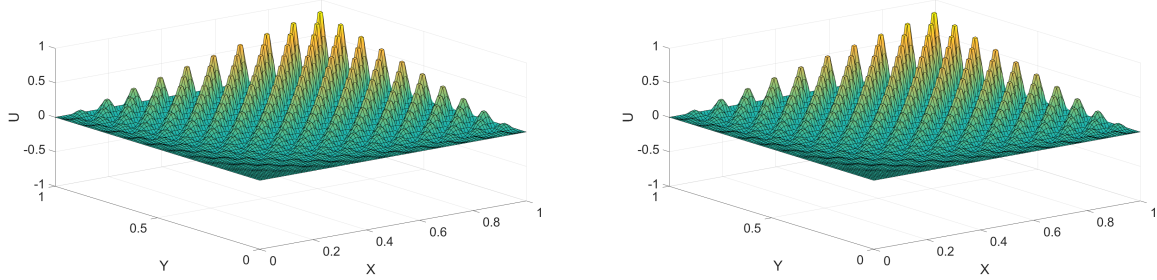
FIGURE 20 2D Diffusion case. Left: reference solution. Right: reconstructed solution with 5 modes. Macro domain partitioned with $2 \times 2 = 4$ degrees of freedom.

to zero. To enforce non-vanishing Dirichlet boundary conditions, the first modes will satisfy the Dirichlet boundary conditions whereas the subsequent modes will be computed with vanishing boundary conditions, following the standard rationale of the PGD [16].

Fig. 20 shows the reference solution for the diffusion case (left) versus the reconstructed solution using 5 modes of the PGD. The macro domain has been partitioned using a mesh of 4 nodes per direction but since the nodes at the boundary are set to zero, the final degrees of freedom are $2 \times 2 = 4$. Note that there is no perceivable difference between the reference solution and the reconstructed one.

Fig. 21 shows both the relative error with respect to the reference solution (left) and the L2 norm of each PGD mode (right) for the 2D diffusion case. The method converges towards the reference solution and the proposed methodology is also able to extract the multi-scale PGD modes ordered in decreasing norm. Therefore, a stopping criterion based on the mode weight seems suitable for this case.

Fig. 22 shows the convergence of the alternated direction algorithm for each one of the modes in the diffusion case. All modes are converging until the desired fixed point accuracy.
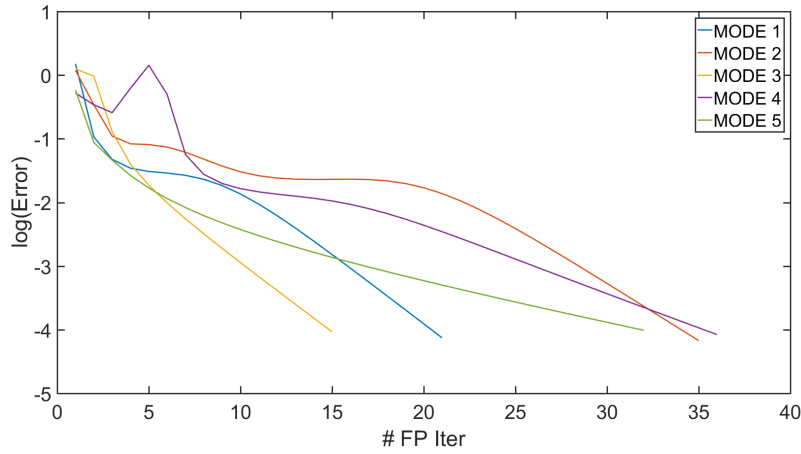
3.5 | 2D convection-diffusion problem

The weak form associated with this diffusion problem is

$$\int_\Omega w^*(\mathbf{x}, \tau_x, \tau_y) \frac{Du(\mathbf{x}, \tau_x, \tau_y)}{Dy} d\mathbf{x} + \int_\Omega \frac{Dw^*(\mathbf{x}, \tau_x, \tau_y)}{Dx} \frac{Du(\mathbf{x}, \tau_x, \tau_y)}{Dx} d\mathbf{x} = \int_\Omega w^*(\mathbf{x}, \tau_x, \tau_y) f(\mathbf{x}) d\mathbf{x}, \quad \forall \, \mathbf{x} \in \Omega = [0, 1]^2 \quad (27)$$
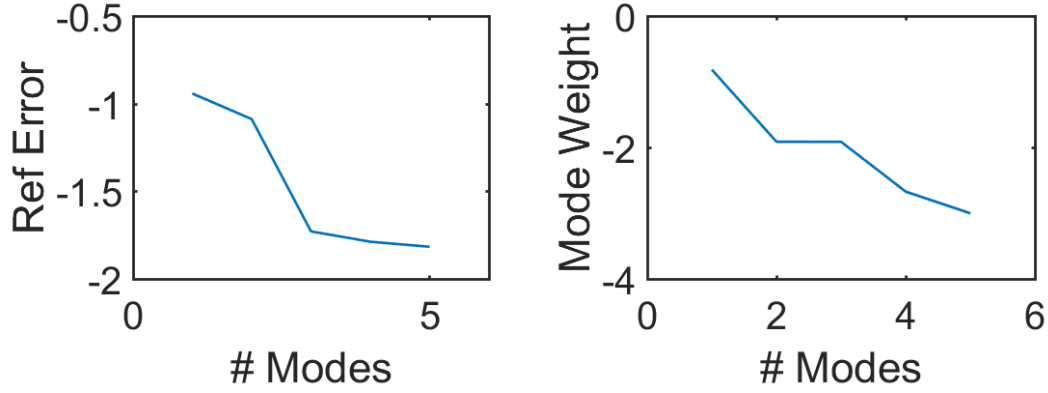
FIGURE 21 2D Diffusion case. Left, L2 relative error of the reconstructed solution with respect to the reference solution. Right, L2 norm for each multi-scale PGD modes.

FIGURE 22 Alternate direction scheme convergence for the 2D diffusion case.

Note that along the y direction there is a pure convection phenomenon, whereas the x direction presents pure diffusion. Hence, the nature of the PDE forces to impose boundary conditions at both ends of the x interval, whereas only initial boundary conditions must be imposed in the y direction. The source term reads in this case

$$f(\mathbf{x}) = (16w^2y^2 + 2y)\sin(4wx) + (64w^2 + w)\sin(8wx)\sin(wy) \tag{28}$$

while the set of boundary conditions ensuring the well-posedness of the problem reads

$$u(0, y) = u(1, y) = u(x, 0) = 0. \tag{29}$$

In this case the angular velocity is set to $w = \pi$.

Under this set of conditions, the partial differential equation (27) admits a unique solution given by

$$u(\mathbf{x}) = \sin(4wx)y^2 + \sin(8wx)\sin(wy). \tag{30}$$

Fig. 23 shows the reference solution (left) versus the reconstructed solution involving 5 modes (right). The macro domain has been partitioned using $3 \times 4 = 12$ degrees of freedom. As it can be noticed, the reconstructed solution already captures the main features of the reference solution. It is important to notice how the reconstructed solution is able to reproduce the set of homogeneous boundary conditions imposed in the 3 sides of the squared domain.
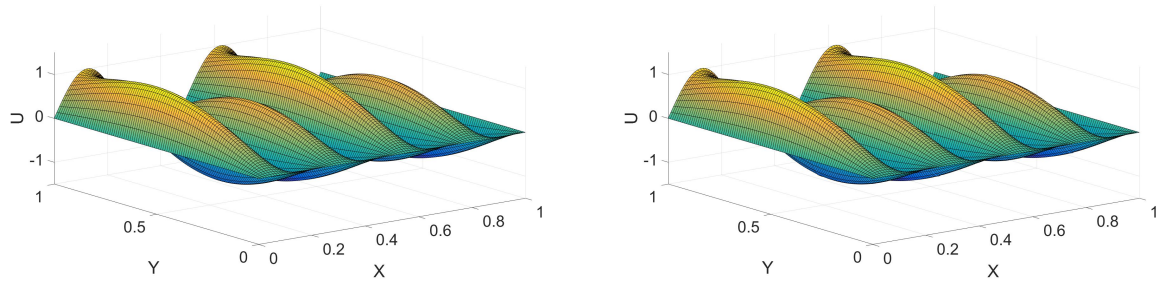
FIGURE 23 2D Convection-Diffusion case. Left: reference solution. Right: reconstructed solution with 5 modes. Macro domain partitioned with $3 \times 4 = 12$ degrees of freedom.
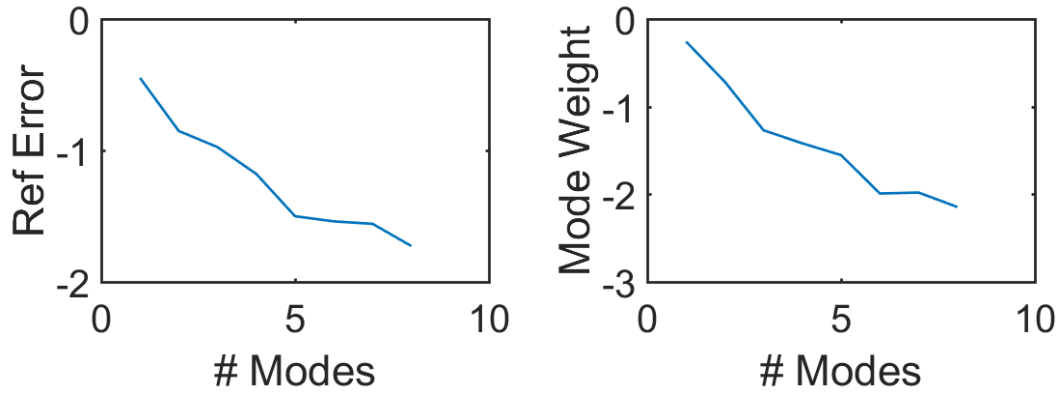
FIGURE 24 2D Convection-Diffusion case. Left, L2 relative error of the reconstructed solution with respect to the reference solution. Right, L2 norm for each multi-scale PGD modes.

Fig. 24 left shows the relative error versus the number of modes involved in the reconstructed solution for the convection diffusion case. Right subplot depicts the L2 norm of each PGD mode involved in the approximation. The error decreases with respect to the number of modes, showing good convergence properties even for convection diffusion problems. Moreover, the norm of each PGD mode tends to decrease as more PGD modes are involved in the solution.

Fig. 25 shows the convergence of the alternated direction algorithm for each one of the modes in the convection diffusion case. It can be appreciated how all modes are converging, yet compared with the pure diffusive case some modes present slower convergence.

3.6 | Transient Thermal Problem with Multi-Scale material operator.

The previous 2D convection diffusion case was the prequel to a more elaborated problem with multi-scale material operator. Let us consider a thermal transient problem (time is seen as an extra coordinate) of a 1D bar. If the material properties are homogeneous, the PDE controlling the process is identical to the one studied in the previous convection-diffusion case. However, we are interested in exploring the performance of the methodology when the material parameters also present some variation along the physical space.

Fig. 26 shows two test cases where the material parameter presents a variation in the spatial domain. The first one consists of 4 thick inclusions, whereas the second one is based on 16 thin inclusions.

Since no reference solution is available in this particular case, a reference solution has been computed using full FEM approximation for the entire space-time domain. The mesh used in the 4-inclusion case consists of 6400 linear elements whereas the one employed in the 16-inclusion case has 9216 elements. The macro domain is partitioned the same way than in the previous convection diffusion case having 12 total degrees of freedom (3 dofs in the space domain times 4 dofs in the time domain).
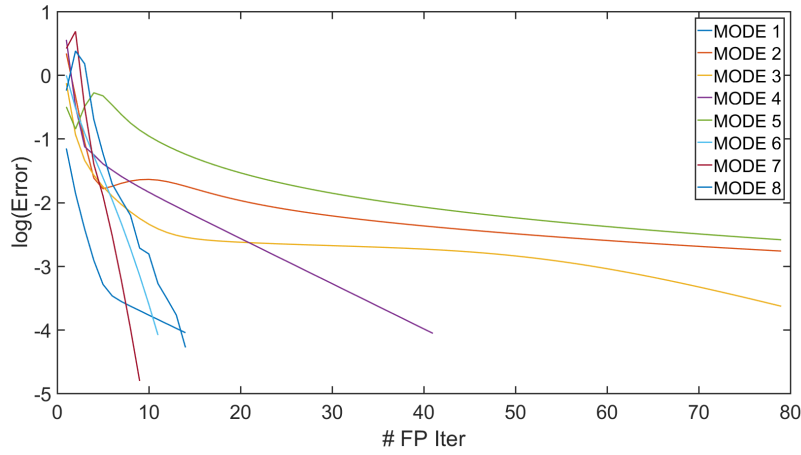
FIGURE 25 Alternate direction scheme convergence for the 2D convection-diffusion case.
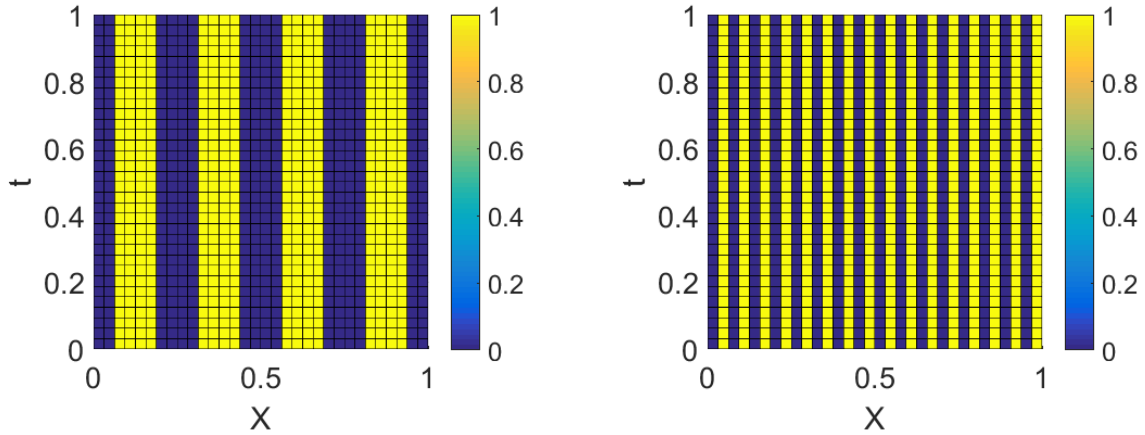
FIGURE 26 Thermal conductivity of the 1D bar in the space-time domain. Yellow, material A, conductivity equal to 10. Blue, material B, conductivity equal to 1.

Each micro-scale unidimensional mode is discretized using 80 piecewise linear elements. The forcing is the same than the one presented in the previous convection-diffusion case as well.

3.6.1 | 4-inclusion case.

Fig. 27 shows the space-time solution for the 4 inclusions transient heat problem when using full FEM discretization (left) and multi-scale PGD approximation (right). Almost no difference can be appreciate between the full FEM discretization and the multi-scale PGD approximation when using 8 modes. Note how the derivate of the solution along the space direction is smaller in regions where the material conductivity is higher (yellow material).

Fig. 28 shows the convergence of the multi-scale PGD towards the full FEM approximation as the number of modes increases (right). Moreover, there exists an important decay of the mode weight as more modes are added to the solution.

Fig. 29 shows the convergence of the alternated direction algorithm for each one of the modes for the 4 inclusions case. It can be appreciated how all modes are converging, yet some modes require few tens of fixed point iterations to converge up to the desired tolerance.
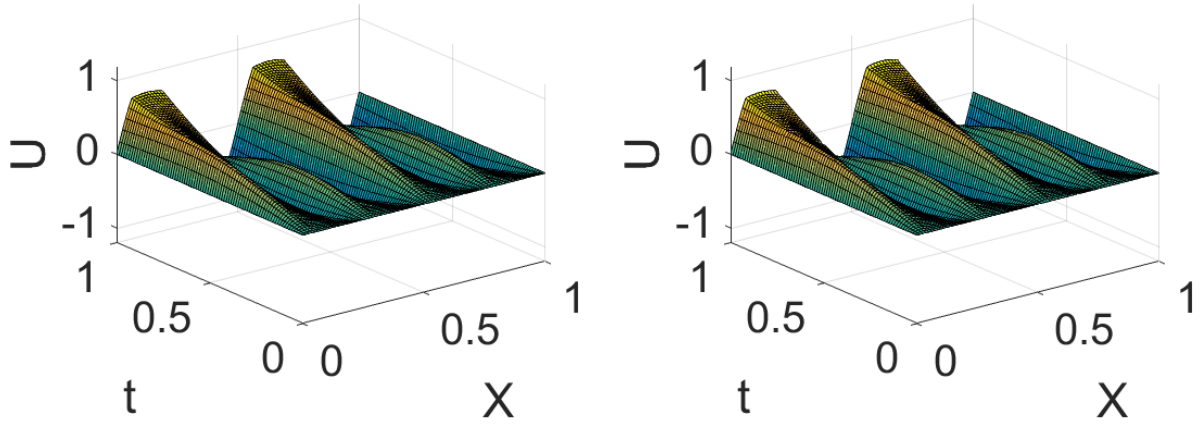
FIGURE 27 4 Inclusions transient thermal problem case. Left: full FEM reference solution. Right: reconstructed solution with 8 modes. Macro domain partitioned with $3 \times 4 = 12$ degrees of freedom.
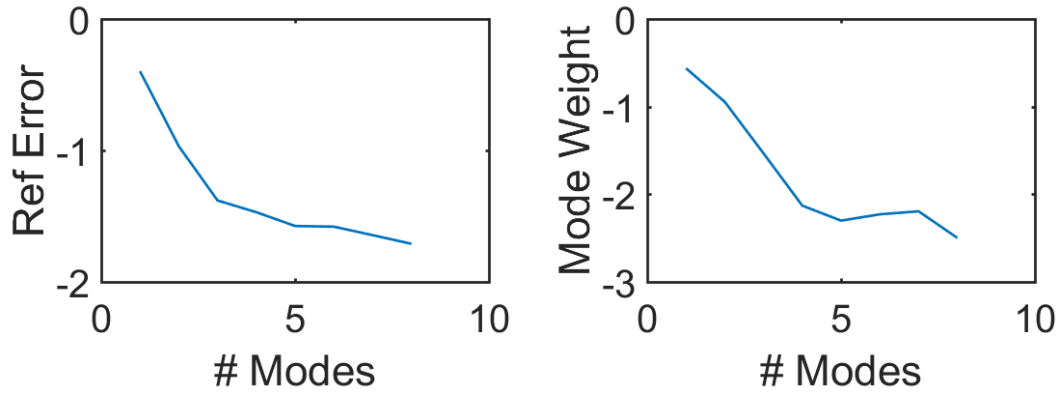

FIGURE 28 4 Inclusions transient thermal case. Left, L2 relative error of the reconstructed solution with respect to the reference solution. Right, L2 norm for each multi-scale PGD modes.

In the multiscale context, it is important to use other norms to measure the quality of the solution appart from the standard L_2 norm. Indeed, capturing effectively the derivatives of the solution is a major concern for multi-scale media. Eqs. 31 and 32 show the H_1 norm just like the relative H_1 error used in this particular case.

$$||u||_{H1} = \int_\Omega u^2 d\Omega + \int_\Omega \nabla u \cdot \nabla u d\Omega \tag{31}$$

$$\mathcal{E}_{H1} = \frac{||u - u_{ref}||_{H1}}{||u_{ref}||_{H1}} \tag{32}$$

Fig. 30 shows the H_1-error convergence in logarithmic scale for different PGD modes. As it can be seen, the error is monotonicly decreasing when increasing the number of PGD modes. However, it is important to acknowledge that capturing derivatives within the PGD framework normally requires more enrichments (or modes) that the ones required to capture the primal variable. Or in other words, a small error in the primal variable may be amplified in the dual variable involving derivatives. Therefore, we would expect that the H_1 norm presents slower convergence results than the L_2 indicator for more complicated scenarios.
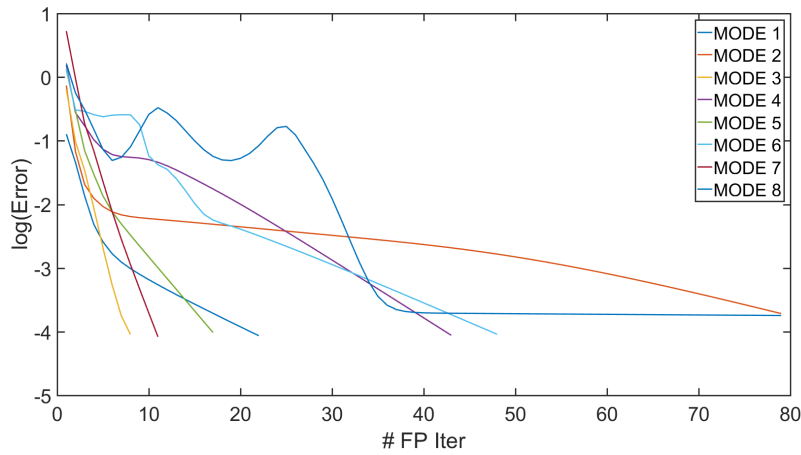
FIGURE 29 Alternate direction scheme convergence for the 4 inclusions transient heat case.
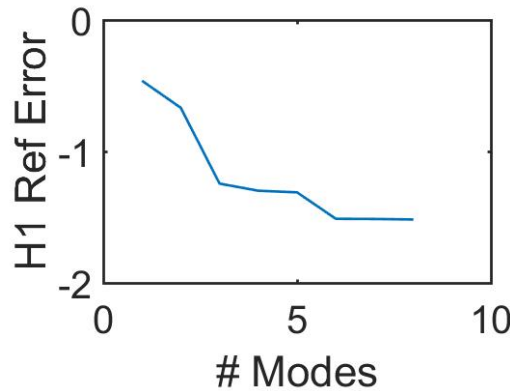

FIGURE 30 H_1 error convergence in logarithmic scale for the 4 inclusions transient heat case.
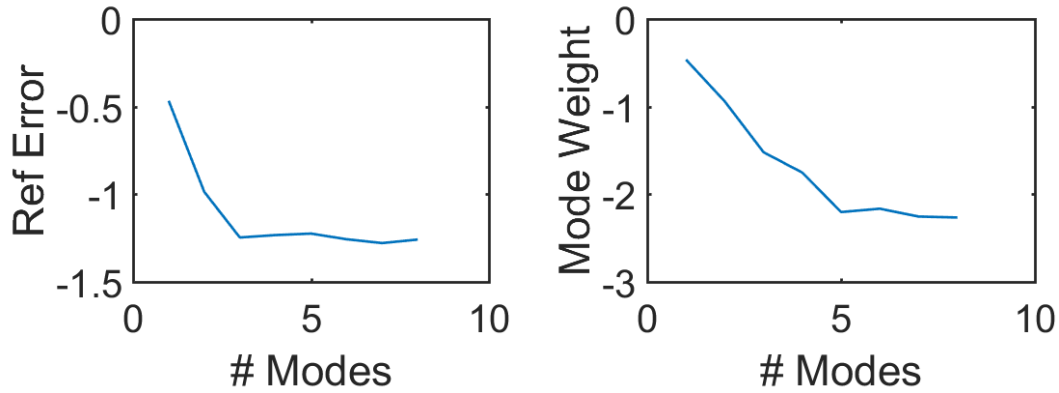
3.6.2 | 16-inclusion case.

The same analysis for the 16-Inclusion than the one performed for the 4-inclusion case is studied in this section. Fig. 31 shows the space-time solution for the 16-inclusion transient heat problem when using full FEM discretization (left) and multi-scale PGD approximation (right). The effect of the highly varying material parameter can be easily appreciated in the solution. The solution presents plenty of high slopes in the vicinity of the material interfaces. The PGD is in good agreement with the full FEM solution, even though small perturbations are appearing at the interface between macro elements. This fact is arising from the fact that the solution is highly non-linear at each macro patch, and thus, the multi-scale methodology would require more modes to converge as the micro-scale modes may be very different for each macro nodes.

Fig. 32 shows the convergence of the multi-scale PGD towards the full FEM approximation as the number of modes increases (right) for the 16-Inclusions case. The convergence towards the reference solution is slower than the 4-inclusion case. This worsening convergence could be easily explained when considering the following two facts. The first one comes from the fact that the same macro mesh has been employed for the 4-inclusion and 16-inclusion cases. As a consequence, the solution that each individual PGD patch has to replicate is more complicated in the 16-inclusions case compared to the 4-inclusions case, ultimately requiring more modes. The second issue arises from the fact each separated micro functions is replicated throughout the entire domain, being weighted by the macro-scale nodes. Indeed, it is fair to reckon that the less reciprocity between different PGD patches will lead to an increment in the number of micro scale separated functions (or modes) to capture the solution. That
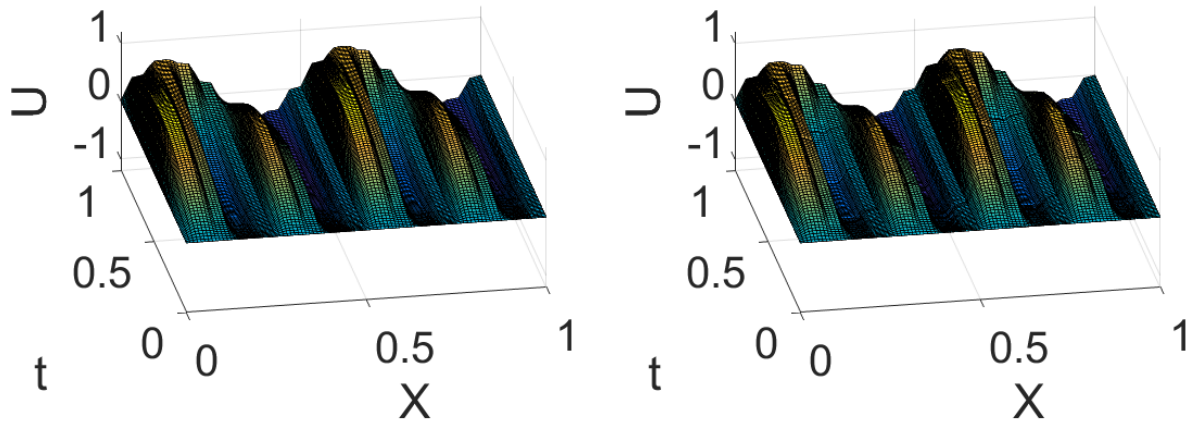
FIGURE 31 16 Inclusions transient thermal problem case. Left: full FEM reference solution. Right: reconstructed solution with 8 modes. Macro domain partitioned with $3 \times 4 = 12$ degrees of freedom.

FIGURE 32 16-inclusion transient thermal case. Left, L2 relative error of the reconstructed solution with respect to the reference solution. Right, L2 norm for each multi-scale PGD modes.

said, another valuable route is to consider a finer macro-partition for the 16-inclusion case, being aware that it will require less number of modes but the price to compute one mode will increase.

As mentioned before, since each local micro-scale path has to replicate a very different non-linear behavior, it is reasonable to expect that the multi-scale PGD methodology will require more modes to converge to the solution.

Fig. 33 shows the convergence of the alternated direction algorithm for each one of the modes for the 16-inclusion case. It can be appreciated how all modes are converging and some modes require few fixed point iterations to converge up to the desired tolerance.

3.7 | Time Multi-Scale applied to a discrete system of equations

The main aim of this example is to show the capabilities of the algorithm to predict the response of a transient system of equations arising from a standard FEM discretization in space. The strong form of the problem reads

$$\frac{\partial u(x,t)}{\partial t} - \frac{\partial^2 u(x,t)}{\partial x^2} = f(x,t). \tag{33}$$
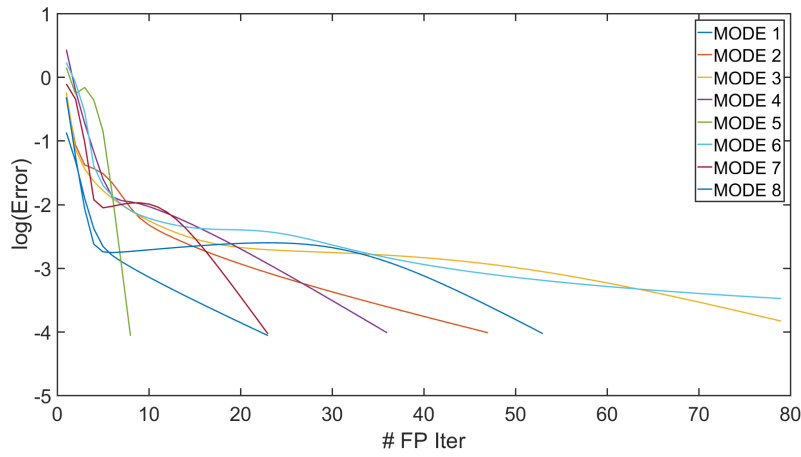
FIGURE 33 Alternate direction scheme convergence for the 16 inclusions transient heat case.
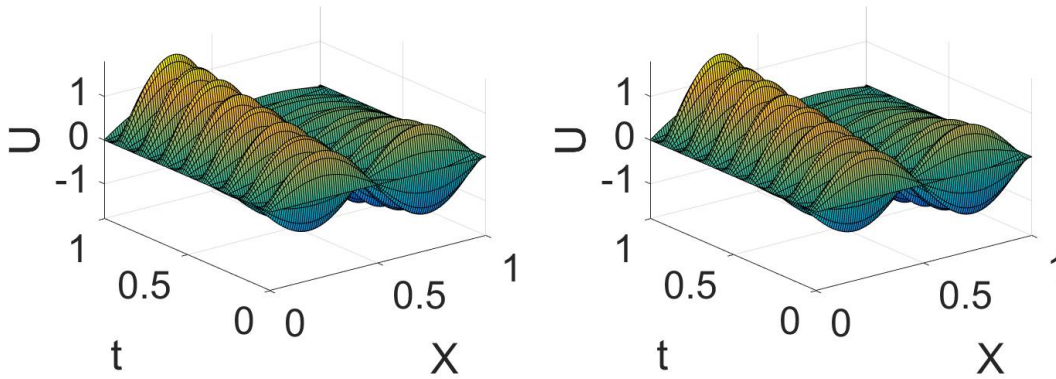
FIGURE 34 Discrete case. Reference solution, left. Reconstructed solution with 3 modes, right. Temporal domain partitioned with 4 macro degrees of freedom.

Indeed, the problem analyzed in this section makes reference to a 1D transient thermal problem subjected to the following boundary conditions and source term

$$f(x,t) = (4\pi^2(sin(t) + sin(50t)) + cos(t) + 50cos(50t))sin(2\pi x)$$
$$u(x,0) = 0$$
$$u(0,t) = u(1,t) = 0 \tag{34}$$

This partial differential equation under this set of boundary conditions admits an analytical solution

$$u(x,t) = (sin(t) + sin(50t))sin(2\pi x), \tag{35}$$

which presents a two scale behavior in the time domain.

If the spatial 1D domain is discretized using 80 linear elements equally spaced, it gives the discrete system of equations

$$\mathbf{M\dot{u}}(t) + \mathbf{Ku}(t) = \mathbf{f}(t) \in t = [0,T], \tag{36}$$

where multi-scale is applied only in time.

Fig. 34 shows the reference solution (left) and the reconstructed solution (right) using 3 mode for the discretized transient thermal problem. As it can be noticed, the obtained solution is in good agreement even when involving only one mode. This
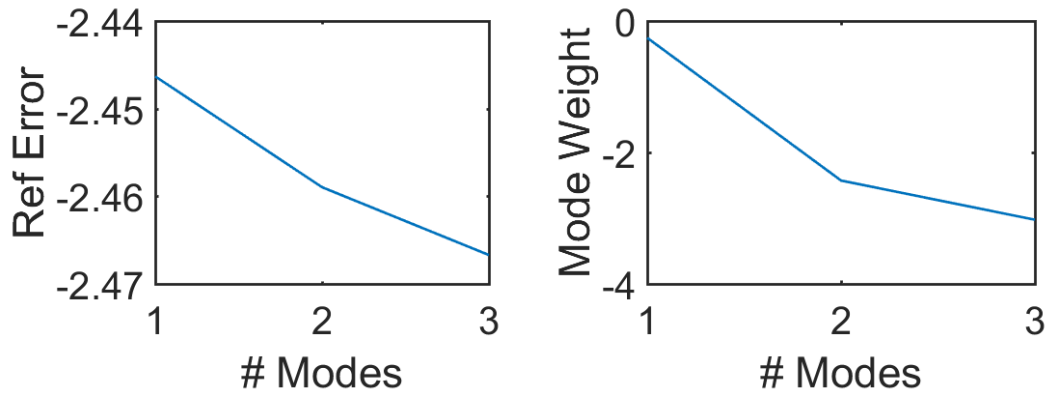
FIGURE 35 Discretized transient problem. Left, L2 relative error of the reconstructed solution with respect to the reference solution. Right, L2 norm for each multi-scale PGD modes.

FIGURE 36 Alternate direction scheme convergence for the spatially discretized transient system.

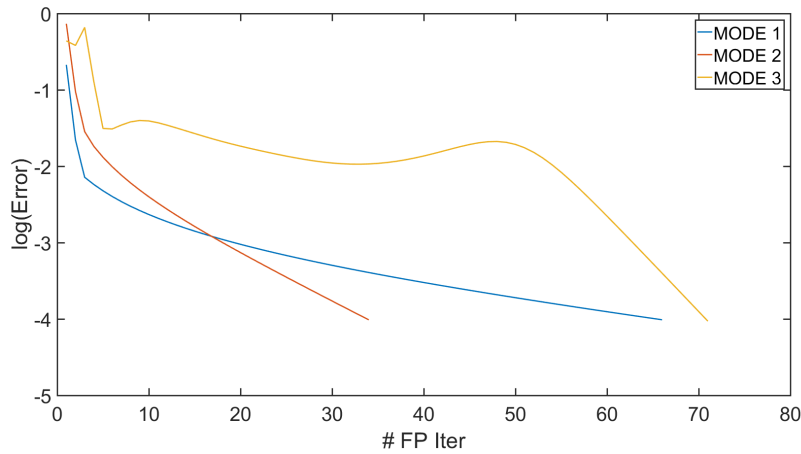fact is not surprising since the analytical solution composed by three separated modes involves produces a relative error with respect to the analytical solution of $1e - 2.4$ as shown in Fig. 35 .

The convergence of the alternate direction scheme for this discretized transient problem is shown in Fig. 36 . As it can be seen, the fixed point procedure reaches the stopping criteria for the three PGD modes composing the solution.

4 | CONCLUSIONS

A novel algorithm able to solve multi-scale problems in an efficient way is proposed in this work. The algorithm combines a macro partition of the domain which is enriched within the PU rationale. The resulting multi-scale multi-dimensional model is solved using the PGD separated representation. The convergence of the algorithm is proven to be very effective for 1D and 2D problems, involving algebraic, diffusion and convection phenomena.

The methodology renders good results even when the macro domain partition does not involve a pure periodical signal in the micro scale. The extension of the algorithm to higher dimensional spaces is our current line of research just like the extension of the methodology to non-rectangular domains.

☐

APPENDIX

A ELEMENTAL OPERATORS

The main aim of the appendix is to give details about the construction of the operators required to make the multi-scale PGD approximation for the different two-dimensional PDEs analyzed in the paper. It is worth to mention that the potential of the PGD algorithm is achieved when all expressions appearing in the formulation are separable. Therefore, we will assume that the macro shape functions appearing in a 2D problem are separable,

$$N_i(x, y) = N_i^x(x)N_i^y(y). \tag{A1}$$

Note that this is the case, for instance, of linear rectangular elements. Nevertheless, the methodology could be applied to more complex elements, involving more terms in the separation of the shape function.

A.1 Diffusive Operator

In this subsection a diffusion of a scalar field $u(x, y)$ along the x direction is developed. The derivation for the diffusion along the y direction follows a similar rationale. For the sake of simplicity but without loosing generality, we will also assume that a new mode in the macro direction is desired. Therefore, all variations related to the micro x and y direction are set to zero.

$$
\int_{\Omega_e} \frac{Du^*}{Dx} \frac{Du}{Dx} dx dy = \sum_{i=1}^{4} \sum_{j=1}^{4} \sum_{k=1}^{M} \int_{\Omega_e} u_i^* \left(\frac{\partial N_i}{\partial x} X_M Y_M + N_i \frac{\partial X_M}{\partial x} Y_M \right) \left(\frac{\partial N_j}{\partial x} X_k Y_k + N_j \frac{\partial X_k}{\partial x} Y_k \right) u_j dx dy
$$

$$
= \sum_{i=1}^{4} \sum_{j=1}^{4} \sum_{k=1}^{M} u_i^* u_j \int_x X_M \frac{\partial N_i^x}{\partial x} \frac{\partial N_j^x}{\partial x} X_k dx \int_y Y_M N_i^y N_j^y Y_k dy
$$

$$
+ \sum_{i=1}^{4} \sum_{j=1}^{4} \sum_{k=1}^{M} u_i^* u_j \int_x \frac{\partial X_M}{\partial x} N_i^x \frac{\partial N_j^x}{\partial x} X_k dx \int_y Y_M N_i^y N_j^y Y_k dy
$$

$$
+ \sum_{i=1}^{4} \sum_{j=1}^{4} \sum_{k=1}^{M} u_i^* u_j \int_x \frac{\partial X_M}{\partial x} N_i^x N_j^x \frac{\partial X_k}{\partial x} dx \int_y Y_M N_i^y N_j^y Y_k dy
$$

$$
+ \sum_{i=1}^{4} \sum_{j=1}^{4} \sum_{k=1}^{M} u_i^* u_j \int_x X_M \frac{\partial N_i^x}{\partial x} N_j^x \frac{\partial X_k}{\partial x} dx \int_y Y_M N_i^y N_j^y Y_k dy \tag{A2}
$$

It can be highlighted that four different contributions are appearing due to the application of the chain rule. Furthermore, all terms appearing in the last part of Eq. ($A2$) already present a separated format.

A.2 Convective Operator

In this subsection a pure convection of a scalar field $u(x, y)$ along the x direction is derived. It is important to notice that this case is a particular case of a general convection given by the velocity field $\mathbf{v}$, where a separated representation of the velocity field would be required. The derivation for the convection along the y direction is given as an exercise for the reader. For the sake of simplicity but without loosing generality, we will also assume that a new mode in the macro direction is desired, being the micro scale directions known.

$$\int_{\Omega_e} u^* \frac{\partial u}{\partial x} dx dy = \sum_{i=1}^{4} \sum_{j=1}^{4} \sum_{k=1}^{M} \int_{\Omega_e} u_i^* N_i X_M Y_M \left(\frac{\partial N_j}{\partial x} X_k Y_k + N_j \frac{\partial X_k}{\partial x} Y_k \right) u_j dx dy$$

$$= \sum_{i=1}^{4} \sum_{j=1}^{4} \sum_{k=1}^{M} u_i^* u_j \int_x X_M N_i^x \frac{\partial N_j^x}{\partial x} X_k dx \int_y Y_M N_i^y N_j^y Y_k dy$$

$$+ \sum_{i=1}^{4} \sum_{j=1}^{4} \sum_{k=1}^{M} u_i^* u_j \int_x X_M N_i^x N_j^x \frac{\partial X_k}{\partial x} dx \int_y Y_M N_i^y N_j^y Y_k dy. \quad (A3)$$

Once again all integrals appearing in the last part of Eq. (A3) are written already in a separated way, improving the efficiency of the algorithm.

References

1. A. Abdulle and Y. Bai. *Reduced basis finite element heterogeneous multi-scale method for high-order discretizations of elliptic homogenization problems*. Journal of Computational Physics 2012; 231:7014-7036

2. A. Ammar, F. Chinesta, E. Cueto and M. Doblare. *Proper generalized decomposition of time-multiscale models*. International Journal for Numerical Methods in Engineering, vol. 90, pp. 569-596, 2012.

3. I. Babuška and J. M. Melenk. The partition of unity method. International journal for numerical methods in engineering 40.4 (1997): 727-758.

4. A. Badias, D. Gonzalez, I. Alfaro, F. Chinesta and E. Cueto. *Local Proper Generalized Decomposition*. Numerical Methods in Engineering, vol. 112, 2017.

5. S. Boyaval *Reduced-basis approach for homogenization beyond the periodic setting*. Multiscale Modeling and Simulation 2008; 7(1):466-494

6. F. Chinesta, G. Chaidron and A. Poitou. *On the Solution of the Fokker-Planck Equations in Steady Recirculating Flows Involving Short Fiber Suspensions*. Journal of Non-Newtonian Fluid Mechanics, vol. 113, pp. 97-125, 2003.

7. M. Chevreuil, A. Nouy and E. Safatly. *A multiscale method with patch for the solution of stochastic partial differential equations with localized uncertainties*. Computer Methods in Applied Mechanics and Engineering 2013; 255:255-274

8. F. Chinesta, A. Leygue, F. Bordeu, J.V. Aguado, E. Cueto, D. Gonzalez, I. Alfaro, A. Ammar and A. Huerta. *PGD-Based Computational Vademecum for Efficient Design, Optimization and Control.*. Archives of Computational Methods in Engineering, vol. 20, pp. 31-59, 2013.

9. F. Chinesta, P. Ladevèze, and E. Cueto. *A short review on model order reduction based on proper generalized decomposition.* Archives of Computational Methods in Engineering 18, no. 4, 395, 2011.

10. F. Chinesta and E. Cueto. *PGD-based modeling of materials, structures and processes*. Heidelberg: Springer, 2014.

11. E. Cueto, D. Gonzalez and I. Alfaro. *Proper generalized decompositions: an introduction to computer implementation with Matlab*. Springer, 2016.

12. J. Donea and A. Huerta. *Finite element methods for flow problems*. John Wiley & Sons, 2003.

13. Y. Efendiev, J. Galvis and F. Thomines. *A systematic coarse-scale model reduction technique for parameter-dependent flows in highly heterogeneous media and its applications*. Multiscale Modeling and Simulation 2012; 10(4):1317-1343

14. F. Feyel. *Multiscale FE^2 elastoviscoplastic analysis of composite structures.* Computational Materials Science 1999; 16(1?4):344–354.

15. F. Fritzen and M. Leuschner. *Reduced basis hybrid computational homogenization based on a mixed incremental formulation.* Computer Methods in Applied Mechanics and Engineering 260 (2013): 143-154.

16. D. Gonzalez, A. Ammar, F. Chinesta, and E. Cueto. *Recent advances on the use of separated representations.* International Journal for Numerical Methods in Engineering 81, no. 5, pp. 637-659, 2011.

17. D. Gonzalez, E. Cueto, F. Chinesta, P. Diez and A. Huerta. *SUPG-based stabilization of Proper Generalized Decompositions for high-dimensional advection-diffusion equations.* Int. J. Numer. Methods Eng 94, no. 13, pp. 1216-1232, 2013.

18. R. Ibáñez, E. Abisset-Chavanne, F. Chinesta, A. Huerta and E. Cueto. *A local, multiple Proper Generalized Decomposition based on the Partition of Unity.* International Journal of Numerical Methods in Engineering, submitted, 2018.

19. Y. Maday and G. Turinici. *A parareal in time procedure for the control of partial differential equations.* Comptes Rendus Mathematique 335.4 (2002): 387-392.

20. J. M. Melenk and I. Babuška. *The partition of unity finite element method: basic theory and applications.* Computer methods in applied mechanics and engineering 139.1-4 (1996): 289-314.

21. J.C. Michel, H. Moulinec and P. Suquet. *Effective properties of composite materials with periodic microstructure: a computational approach.* Computer methods in applied mechanics and engineering, vol. 172, pp. 109-143, 1999.

22. D. Néron and P. Ladevèze. Proper generalized decomposition for multiscale and multiphysics problems. Archives of Computational Methods in Engineering 17.4 (2010): 351-372.

23. S. Niroomandi, I. Alfaro, D. Gonzalez, E. Cueto and F. Chinesta. *Model order reduction in hyperelasticity: a Proper Generalized Decomposition approach.* International Journal for Numerical Methods in Engineering, vol. 00, pp. 1-28, 2012.

24. U. Trottenberg, C. W. Oosterlee and A. Schuller. Multigrid. Elsevier, 2000.

25. F. Fritzen and M. R. Hassani. *Space-time model order reduction for nonlinear viscoelastic systems subjected to long-term loading.* Meccanica. 10.1007/s11012-017-0734-x, 2017.

26. JC. Passieux, P. Ladevèze, D. Néron. *A scalable time-space multiscale domain decomposition method: adaptive time scale separation.* Computational Mechanics. https://doi.org/10.1007/s00466-010-0504-2, 2010.

27. Y. Maday, M. Riahi and J. Salomon. *Parareal in Time Intermediate Targets Methods for Optimal Control Problems.* Control and optimization with PDE constraints. Based on the international workshop on control and optimization of PDEs, Mariatrost, Austria, 2011.

28. T. Hughes, G. Feijóo, L. Mazzei and J.B. Quincy. *The variational multiscale method: a paradigm for computational mechanics.* Computer Methods in Applied Mechanics and Engineering, vol. 166, pp. 3-24, 1998.

29. R. Codina, S. Badia, J. Baiges and J. Principe. *Variational Multiscale Methods in Computational Fluid Dynamics.* https://doi.org/10.1002/9781119176817.ecm2117, 2017.

30. I. Babuska and J.M. Melenk *The Partition of Unity Method.* International Journal for Numerical Methods in Engineering, vol. 40, pp. 727-758, 1997.